Numerical Investigation on Condensation of Non-Condensable Gas in Large Deformation Enhanced Tube

Yuanhui Zhang[1], Ting Zheng[1,*] and Xuegang Zhang[2]

[1] School of Intelligent Manufacturing and Automotive Engineering, Luzhou Vocational and Technical College, Luzhou, 646000, China

[2] School of Intelligent Manufacturing, Panzhihua University, Panzhihua, 617000, China

INFORMATION

Keywords:
Large deformation heat transfer tube
non-condensable gas
condensation heat transfer
numerical investigation

DOI: 10.23967/j.rimni.2025.10.69517

Revista Internacional de Métodos Numéricos para Cálculo y Diseño en Ingeniería

RIMNI

Numerical Investigation on Condensation of Non-Condensable Gas in Large Deformation Enhanced Tube

Yuanhui Zhang[1], **Ting Zheng**[1,*] **and Xuegang Zhang**[2]

[1]School of Intelligent Manufacturing and Automotive Engineering, Luzhou Vocational and Technical College, Luzhou, 646000, China

[2]School of Intelligent Manufacturing, Panzhihua University, Panzhihua, 617000, China

ABSTRACT

In order to improve the condensation heat transfer performance of tube-lines in cooling systems, a new type of large deformation heat transfer tube was proposed. Based on the theory of diffusion, the distributions of temperature, velocity, heat transfer coefficient, and species are presented to compare with smooth tubes. In addition, the effects of relevant parameters on thermo-hydraulic performance are discussed. The numerical results show that the distributions of temperature and velocity show a periodic distribution. The unique structure of the large deformation heat transfer tube disturbs the fluid flow near the wall. The boundary layer of air concentration is destroyed, resulting in heat transfer enhancement. Within the scope of this paper, the heat transfer coefficient and friction factor of the large deformation heat transfer tube are increased by 1.01–3.47 times and 1.05–7.13 times compared with the smooth tube. The heat transfer performance increases with the rising dimple depth and declining non-condensable gas content and dimple pitch.

OPEN ACCESS

Received: 25/06/2025

Accepted: 29/07/2025

Published: 23/01/2026

DOI
10.23967/j.rimni.2025.10.69517

Keywords:
Large deformation heat transfer tube
non-condensable gas
condensation heat transfer
numerical investigation

Nomenclature

$A_{wall\text{-}cell}$	Area of cell on the condensing wall, m^2
D_e	Equivalent diameter, m
D	Diffusion coefficient, m^2·s^{-1}
f	Friction factor
f	Volume force, N
f_0	Friction factor of smooth tubes
F	Surface force, N
g	Gravity, m·s^{-2}
h	Heat transfer coefficient W·m^{-2}·K^{-1}
h_v	Vapor latent enthalpy, J·kg^{-1}
k	Turbulence energy, m^2·s^{-2}

*Correspondence: Ting Zheng (zhengting@lzy.edu.cn).

L	Length of the test section, m
Nu	Nusselt number
Nu_0	Nusselt number of smooth tubes
p	Pressure, Pa
Δp	Pressure drop, Pa
P	Dimple pitch, mm
S	Source term
T	Temperature, K
u	Velocity, m·s^{-1}
y^+	Mesh resolution indicator
$Vcell$	Cell volume, m3

Greek Symbols

ρ	Fluid density, kg·m^{-3}
μ	Dynamic viscosity, Pa·s
μ_t	Turbulent viscosity
λ	Thermal conductivity, W·m^{-1}·K^{-1}
ε	Dissipation rate, m^2·s^{-3}
ω	Mass fraction
Γ	Diffusion coefficient
κ	Effective conductivity
η	Relative error

Subscripts

0	Smooth tube
i	Species i
m	Mass
mom	Momentum
h	Energy

1 Introduction

Steam condensation heat transfer technology is widely used in the electric power, chemical industry, aerospace, and electronic equipment refrigeration [1–3]. However, the phase change process involves a complex heat and mass transfer mechanism. It is important to study the condensation behavior.

Many scholars have studied the process of vapor condensation in heat exchangers [4–6]. Fan et al. conducted an experimental study on natural convection condensation heat transfer outside vertical smooth and corrugated tubes. The temperatures of the crests, valleys, and walls were obtained. The experiment results indicated that the condensation heat transfer coefficient of the corrugated tube was improved by about 10% [7]. Li et al. studied the effects of various enhanced tubes on condensation heat transfer performance by experiment. The experiment results revealed that the corrugated tube presents a better heat transfer performance, and the maximum improvement reaches 27.4% [8].

In engineering applications, the working medium may contain a certain proportion of non-condensable gas (NCG). The NCG has a significant deteriorating effect on heat and mass transfer during the condensation process.

Therefore, it is important to study the enhanced condensation of the steam containing NCG [9,10]. Wu et al. studied the air-steam condensation enhancement in chrome-plated tubes experimentally. The study considered chrome-plated tubes with thicknesses of 1 μm (Tube No. 1) and 10 μm (Tube No. 2). The results indicated that the structure of the chrome-plated tube has a great effect on condensation behavior. The surface of Tube No. 1 was partly condensed in the form of a drop, and the surface of Tube No. 2 was partly condensed in the form of a film [11]. Gong et al. analyzed the condensation process of the steam in a horizontal tube cooled by the falling film evaporation of seawater on the exterior [12]. They developed a model that integrates mixed vapor condensation heat transfer with a distributed parameter model. Su et al. investigated the steam condensation heat transfer performance of a vertical tube containing NCG. The condensation heat transfer coefficient was obtained when the wall subcooling is 27°C∼70°C, and the air mass fraction is 0.10∼0.80 [13]. An experimental study of the effect of wall subcooling on the condensation heat transfer of steam with constant pressure and constant air mass fraction was carried out. Empirical correlations obtained from helium experiments cover 20% of the data. Ahn et al. conducted experiments on steam condensation in a nearly horizontal tube with an inner diameter of 40 mm, inclined downward by 3 degrees [14]. They investigated the effect of non-condensable gases on the local heat transfer coefficient by varying the inlet steam mass flow rate, air mass fraction, and pressure. The results indicated that the air concentration layer near the tube wall significantly hinders condensation in the upper part of the wall. In contrast, it has little impact on the convective heat transfer in the lower part of the wall. Taehwan et al. conducted comparative experimental measurements of the heat transfer coefficient for the condensation of mixed steam in vertical tubes with 16, 20, and 26 mm diameters [15]. On the basis of comparing the experimental results and analyzing the relationships, recommendations are made for the validity interval of the measured relationships [16].

Additionally, many scholars have conducted numerical or experimental studies on the enhanced condensation of steam containing NCG [17]. Currently, research on the condensation process of these gases in profiled tubes is still in its early stages. Most studies focus on single-phase flow of a single working medium inside tubes. In addition, there is a notable lack of research on condensation heat transfer characteristics inside the tube [18,19].

Furthermore, the modeling approach of the shaped tube is an important problem. The heat transfer enhancement of the dimpled tube has been studied by many researchers [20–23]. Most researchers establish the geometry model using 3D software, which results in a large error.

Therefore, a new modeling method is proposed to generate the physical model of a large deformation enhanced tube (ETDP). The flow characteristics and condensation heat transfer performance are studied based on the diffusion boundary layer theory. Additionally, the effects of air mole fraction, dimple depth, and dimple pitch on thermo-hydraulic performance are discussed.

2 Numerical Model

2.1 Geometric Model

The air-steam flows inside the large deformation heat transfer tube, which is obtained by mechanical extrusion molding, and the modeling process is shown in Fig. 1. Fig. 2 shows the geometric model of the fluid domain of the deformation-enhanced tube, with a tube diameter of 20 mm, a tube length of L = 300 mm, a dimple depth of *D*, and a dimple pitch of *P*. The specific geometric parameters and research content are shown in Table 1.

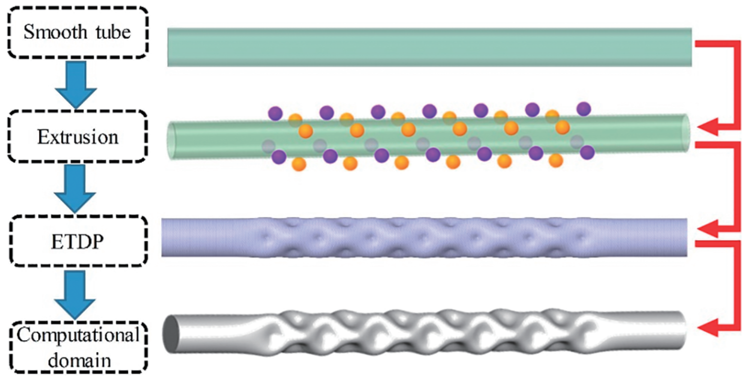

Figure 1: Geometry modeling process of a large deformation enhanced tube

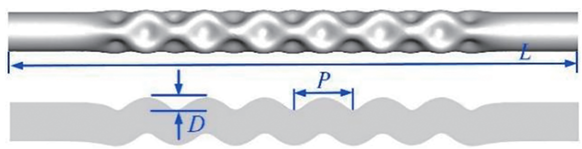

Figure 2: Geometric model of a large deformation enhanced tube

Table 1: Geometric parameters

Chapters	Air mole fraction (%)	Depth of dimples D (mm)	Dimple pitch P (mm)	Note
3.2	10	4	30	Mechanistic study
3.3	10, 30, 50	4	30	Air mole fraction study
3.4	10	2, 3, 4	30	Dimple depth study
3.5	10	4	25, 30, 35	Dimple Pitch Study

2.2 Government Equations

The basic governing equations used for the calculations in this paper are represented below:

Mass Conservation Equation:

$$\nabla \cdot (\rho u) = S_m \tag{1}$$

The energy conservation equation:

$$\nabla \cdot (\rho u u) = \nabla \cdot F + \rho f + S_{mom} \tag{2}$$

Energy conservation equation:

$$\nabla \cdot (\rho u E) = \nabla \cdot (F \cdot u) + \rho f \cdot u + \nabla \cdot (\kappa \nabla T) + S_h \tag{3}$$

Component transport equation:

$$\nabla \cdot (\rho u \omega_i) = \nabla \cdot (\rho D_i \nabla \omega_i) + S_i \tag{4}$$

where ρ is the density; u is the velocity; S_m is the mass source term; F is the surface force; f is the volume force; S_{mom} is the momentum source term; E is the energy; κ is the thermal conductivity; S_h is the energy source term; and the subscript i denotes the gas component.

The turbulence model uses the k-ε realizable model, which is better suited for boundary layer, separation, and recirculation flows that involve rotations and strong backpressure gradients [24].

The transport equations for turbulent kinetic energy as well as dissipation rate are expressed as follows:

$$\frac{\partial}{\partial x_j}\left(\rho k u_j\right) = \frac{\partial}{\partial x_j}\left[\left(\mu + \frac{\mu_t}{\sigma_k}\right)\frac{\partial k}{\partial x_j}\right] + \Gamma - \rho\varepsilon \tag{5}$$

$$\frac{\partial}{\partial x_j}\frac{\partial}{\partial x_j}\left(\rho\varepsilon u_j\right) = \frac{\partial}{\partial x_j}\left[\left(\mu + \frac{\mu_t}{\sigma_\varepsilon}\right)\frac{\partial \varepsilon}{\partial x_j}\right] + C_1\Gamma\varepsilon - C_2\frac{\varepsilon^2}{k + \sqrt{\upsilon\varepsilon}} \tag{6}$$

$$\Gamma = -\overline{u_i u_j}\frac{\partial u_i}{\partial u_j} = \frac{\mu_t}{\rho}\left(\frac{\partial u_i}{\partial x_j} + \frac{\partial u_j}{\partial x_i}\right)\frac{\partial u_i}{\partial x_j} \tag{7}$$

$$C_1 = \max\left[0.43\frac{\mu_t}{\mu_t + 5}\right], C_2 = 1.0, \sigma_k = 1.0, \sigma_\varepsilon = 1.2, \mu_t = \rho C_\mu\frac{k^2}{\varepsilon} \tag{8}$$

2.3 Condensation Model

In this paper, a single-phase multicomponent condensation model is used to numerically simulate the steam-air condensation process. Many scholars have used this numerical model, which has good simulation accuracy for the condensation process of mixed steam containing a high mass fraction of non-condensable gases [25–28]. The use of this numerical model is based on the following assumptions:

1. Vapor-air mixtures have weak intermolecular forces, allowing them to be treated as ideal gases, with all thermophysical properties being a function of temperature.

2. The thermal resistance during condensation primarily arises from non-condensable gases. The main thermal resistance exists in the air concentration boundary layer while the air mass fraction is higher than 20%. Therefore, the thermal resistance of the liquid film can be disregarded, and the condensation wall temperature is considered to be the same as the gas-liquid interface temperature [29,30].

3. Condensation occurs under the condition that the partial pressure of the vapor near the wall is greater than the saturation pressure corresponding to the temperature of the wall, and condensation occurs in the first layer of grid cells close to the condensing wall, and the saturation pressure of the water vapor varies with the temperature by choosing the correlation equation proposed in the literature [30], as follows:

$$P_{sat} = \exp\left[\frac{c_1}{T} + c_2 + c_3 T + c_4 T^2 + c_5 T^3 + c_6 T^4 + c_7 \ln\left(T\right)\right] \tag{9}$$

where $c_1 = -5800.2206$, $c_2 = 1.3914993$, $c_3 = -0.04860239$, $c_4 = 4.1764768\text{e}{-05}$, $c_5 = 1.4452093\text{e}{-08}$, $c_6 = 0$, $c_7 = 6.54259673$.

4. The Effect of Wall Radiation and Wall Suction Is Not Considered

Based on the above assumptions, a three-dimensional single-phase multicomponent transport condensation model is used to describe the mixed steam-air flow near the wall surface of a large deformation-enhanced tube. The condensation process is simulated by adding various source terms to the control equation.

The source terms for the mass of steam as well as air are expressed as follows:

$$S_m = S_v = \frac{\omega_v}{\omega_v - 1}\rho D \frac{\partial \omega_v}{\partial n}\frac{A_{cell-wall}}{V_{cell}} \tag{10}$$

where m is the mass flux, ω_v is the vapor mass fraction, D is the component diffusion coefficient, $\partial\omega_v/\partial n$ indicating the vapor mass fraction gradient at the gas-liquid interface, $A_{cell\text{-}wall}$ is the condensing wall cell area, and V_{cell} is the near-wall cell volume.

The component diffusion coefficient can be calculated by the following equation:

$$D = D_0\left(\frac{P}{P_0}\right)^{-1}\left(\frac{T}{T_0}\right)^{n} \tag{11}$$

where the subscript 0 denotes the standardized state, referring to the relevant literature n takes the value 1.81 [31].

When steam condenses at the wall, the steam is removed in the adjacent cells of the wall, which triggers a change in momentum. The momentum source term in the conservation of momentum equation is calculated by the following equation:

$$S_{mom} = S_{x-mom} + S_{y-mom} + S_{z-mom} = \left(u_x + u_y + u_z\right) S_m \tag{12}$$

The energy source term is the product of the mass source term and the latent heat, as calculated in the following equation:

$$S_h = S_m h_v \tag{13}$$

where h_v is the latent heat of vaporization.

The thermohydraulic performance during condensation is described by the heat transfer coefficient, which characterizes the heat transfer capacity of the wall, and the friction factor, as defined below:

$$h = \frac{\Phi}{A_t\left(T_{wall} - T_m\right)} \tag{14}$$

The coefficient of friction characterizes the pressure loss during flow and is defined below:

$$f = \frac{2\Delta p D_e}{\rho u_i^2 L} \tag{15}$$

where Φ is the heat transfer rate, A_t is the tube wall area, T_{wall} and T_m are the wall and computational domain average temperatures, respectively, Δ_p is the pressure drop, and D_e is the equivalent diameter.

A performance evaluation criterion (PEC) is employed to demonstrate the balance between increasing pressure drop and heat transfer enhancement. The PEC is defined as:

$$PEC = \frac{h/h_0}{f/f_0} \tag{16}$$

2.4 Boundary Conditions and Solution Methods

The background of this study is heat exchangers. The air-steam flows through the tube section, while cooling water flows outside the tubes to cool the steam inside the tubes. In the simulation of steam-air mixture steam condensation in a large deformation-enhanced tube, the inlet is set as a velocity inlet with a velocity range of 1–5 m/s (Re: from 906 to 4057), an initial air volume fraction of 10%, and a steam-air mixture steam temperature of 373 K. The outlet is set as a pressure outlet, and the condensing wall is a thermostatic non-slip wall with $T = 283$ K. The inlet is set as a pressure outlet with a thermostatic non-slip wall. In the simulation, the inlet extension section and the outlet extension section are employed to avoid the entrance effect and backflow. The length of the extension section is 10 times the tube diameter.

In this paper, the finite volume method is utilized to solve the control equations in steady state, and the PISO algorithm is used to solve the coupled solution for pressure and velocity, the discretization format of the pressure correction term is in the second-order format, and the discretization equations for the momentum, turbulent energy, dissipation rate, component and energy equations are in the second-order windward form.

3 Results and Discussion

3.1 Model Validations

In the simulation of mixed vapor condensation within a large deformation-enhanced tube, the fluid domain meshes are used using a hybrid polyhedral-hexahedral mesh, as shown in Fig. 3. In order to better solve the rapidly changing velocities, temperatures, and component concentrations near the wall, the boundary layer mesh is divided for the condensing wall, with the first layer mesh size of 0.05 mm and a growth rate of 1.1, resulting in a total of 10 layers are divided.

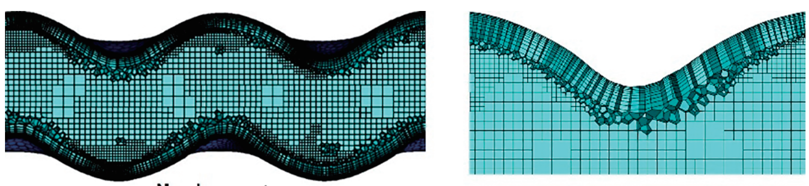

Figure 3: Schematic diagram of the computational domain grid

A standard wall function is selected to accurately simulate the flow structure in the near-wall region. Therefore, the mesh y+ values are controlled to be less than 1. Four sets of meshes with numbers 76859, 156086, 234130, 383279, 709450, and 1220321 were used to verify the mesh-independence, and the results are shown in Table 2. From the figure, it can be seen that when the number of grids rises from 709450 to 1220321, the relative errors of the average heat transfer coefficient and friction factor are 0.13% and 0.77%, respectively. Therefore, the number of grids is chosen to be 709450 for this simulation.

Table 2: Grid-independence test

Mesh system	Grid number	h	Relative error %	f	Relative error %
1	76895	441.5	9.65	0.0415	11.44
2	156086	462	5.45	0.0437	6.74
3	234130	478.79	2.01	0.04555	2.80
4	383279	487.46	0.24	0.04604	1.75

(Continued)

Table 2 (continued)

Mesh system	Grid number	h	Relative error %	f	Relative error %
5	709450	488.01	0.13	0.0465	0.77
6	1220321	488.63	–	0.04686	–

In order to verify the accuracy of the numerical method in this paper, a validation numerical simulation is conducted using the numerical method of this paper. As shown in Fig. 4, the computational domain is simplified to a two-dimensional axisymmetric model. The length of the adiabatic section is 0.81 m, and the length of the condensation section is 2.4 m. The numerical results are compared with the experimental data [32]. The boundary conditions are shown in Table 3. As shown in Fig. 5, the condens the condensing wall temperature boundary condition is fitted as a polynomial function through the experimental data. It can be seen that the error of the centerline temperature is less than 5%. The heat flux has a slightly larger error with the experiment, and the maximum error is about 15%, which may be caused by the smaller air mass fraction and thus affects the calculation accuracy [28]. Therefore, it can be considered that the numerical model proposed in this paper is suitable for the calculation of condensation inside tubes.

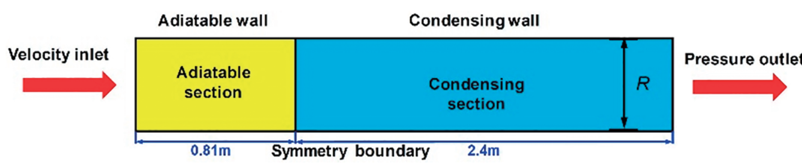

Figure 4: Numerical methods to validate the computational domain

Table 3: Boundary conditions of validation cases

Test	Condition pressure	Inlet temperature	Inlet mass rate	Air mass fraction
Test 1	413.1 KPa	418.45 K	1.667×10^{-2}	0.148
Test 2	420.1 KPa	405.95 K	2.323×10^{-2}	0.376

3.2 Flow Characteristics and Heat Transfer Performance

Fig. 6 shows the distributions of velocity and turbulence kinetic energy (TKE). For the ETDP, the velocity distribution presents a periodic distribution. The mainstream velocity is high, and the velocity is relatively low near the wall. The velocity of ETDP is higher than that of the smooth tube. In addition, the TKE of ETDP is higher than that of the smooth tube, especially in the near-wall region. The deformed wall generates destruction of the boundary layer flow. The fluid mixing between the boundary layer fluid and the mainstream is improved.

Fig. 7 shows the distribution of local air mole fraction and streamline distribution. It reveals that when the air-steam mixture condenses on the wall of the large deformation enhanced tube, the air fraction accumulates near the wall surface, thereby increasing the thermal resistance in the heat transfer process and hindering the steam condensation rate. Due to the unique structure of the deformation-enhanced tube, the fluid is constantly contracting and expanding along the flow direction, thus forming a vortex on the leeward side of the dimple. These vortices disturb the gas flow near the wall, disrupt the air concentration boundary layer, and enhance heat transfer between the steam and the condensing wall. In addition, due to the right-to-left reflux direction of the mixed steam, the fluid located to the left of each notch has a longer residence time, lower flow rate, and higher air volume fraction.

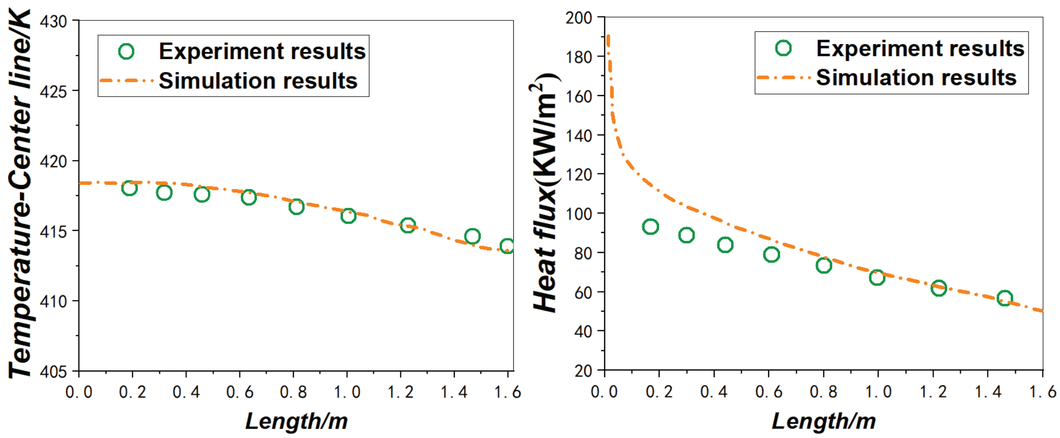

(a) Test 1

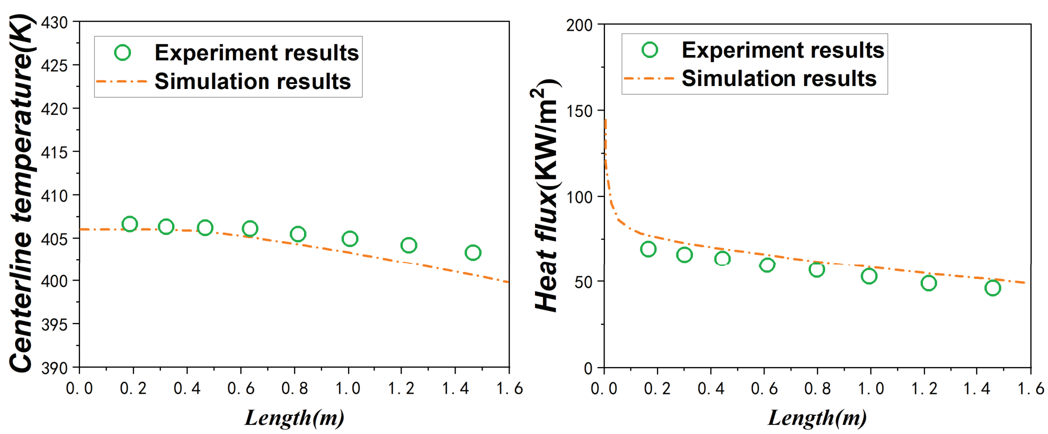

(b) Test 2

Figure 5: Comparison between simulation results and experimental data: (a) test 1 and (b) test 2

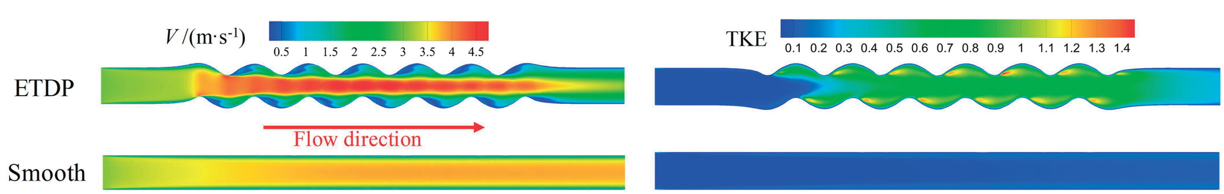

Figure 6: Comparison of velocity and turbulence kinetic energy (TKE)

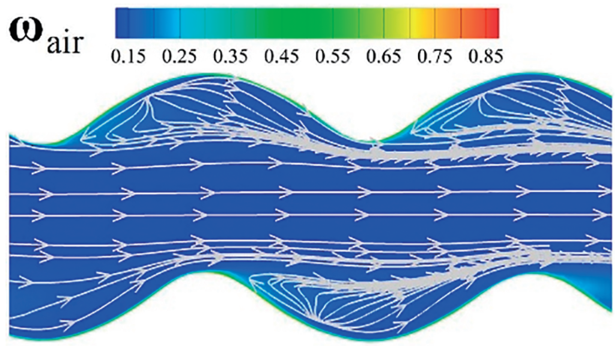

Figure 7: Air volume fraction cloud and local cross-section flow line distribution

As illustrated in Fig. 8, the temperature is highest at the center of the flow domain and decreases near the tube wall, where the mixed vapor continually cools in contact with the condensing surface. At the same time, the low temperature region on the left side inside the bulge is relatively larger due to the presence of vortices inside the tube.

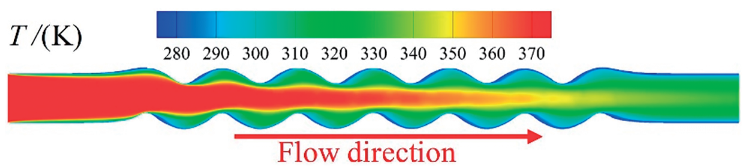

Figure 8: Cross-sectional temperature distribution cloud

Fig. 9 compares the local heat transfer coefficient between the wall of the large deformation enhanced tube and the smooth tube. Overall, the heat transfer coefficient for both types of tubular heat exchanger tubes decreases along the length of the tube, with a more pronounced reduction occurring near the entrance of the tube. The figure demonstrates that the local heat transfer coefficient of the large deformation enhanced tube is higher than that of the smooth tube, suggesting that the large deformation enhanced tube enhances the condensation heat transfer effectiveness compared to the smooth tube. In addition, the local heat transfer coefficient of the large deformation enhanced tube also shows a periodic distribution. The coefficient is relatively high at the apex of each dimple and comparatively low at the apex of the bulges, which is attributed to the fact that the mixed vapors directly hit the windward side of the dimple, effectively destroying the air diffusion boundary layer near the wall, and improving the heat transfer effect.

3.3 Effect of Air Fraction Factor

The variation of average heat transfer coefficient and friction factor is presented in Fig. 10. It can be seen that the heat transfer coefficient increases with increasing velocity, while the friction factor decreases with increasing velocity. As the mole fraction of non-condensable gas increases, the thermal resistance of the air boundary layer becomes larger and the heat transfer coefficient decreases. In addition, the friction factor decreases with the increasing ω_{air}.

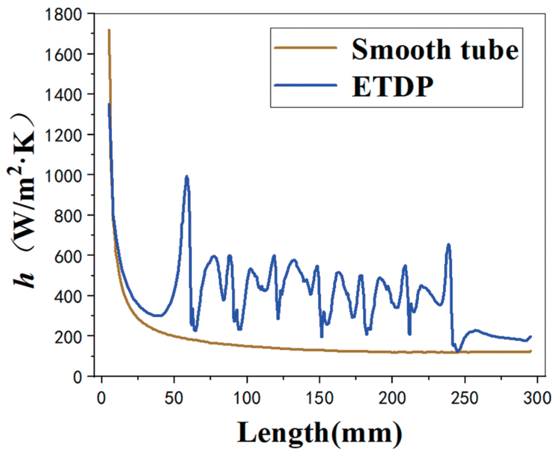

Figure 9: Comparison of local heat transfer coefficient between the large deformation enhanced tube and the smooth tube

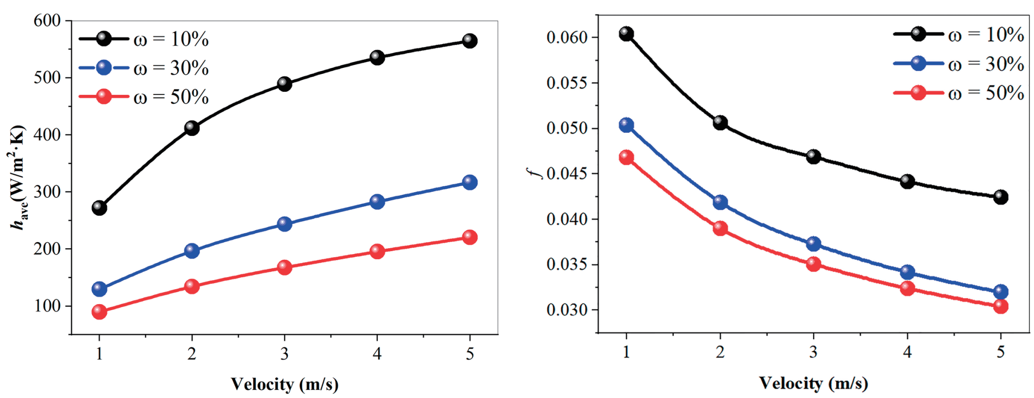

Figure 10: Average heat transfer coefficient and friction factor for different air mole friction

In order to describe the heat transfer enhancement and pressure drop, the dimensionless numbers h/h_0, f/f_0, and PEC are introduced. The trends of h/h_0 and f/f_0 are shown in Fig. 11. It can be seen that the values of h/h_0 and f/f_0 are greater than 1 in all cases, which indicates that the heat transfer performance of the large deformation enhanced tube achieves heat transfer enhancement. Meanwhile, the structure of dimples and protrusions of ETDP increases the pressure drop compared with smooth tubes. The h/h_0 increases with the rising air mole friction. The f/f_0 of $\omega = 10\%$ is higher than that of the other two cases. The maximum of PEC appears at $V = 2$ m/s and $\omega = 10\%$. The maximum value of PEC is 2.1. The PEC of the three cases are close when the velocity reaches 4 m/s. It is revealed that heat transfer enhancement can be achieved by appropriately controlling the air mode fraction.

3.4 Effect of Dimple Depth

Fig. 12 presents the effects of dimple depth on thermo-hydraulic performance. The h/h_0 and f/f_0 increase with the rising dimple depth. The large dimple depth causes a more significant disturbance in the boundary layer flow. The boundary layer flow is disrupted, resulting in improved heat transfer performance.

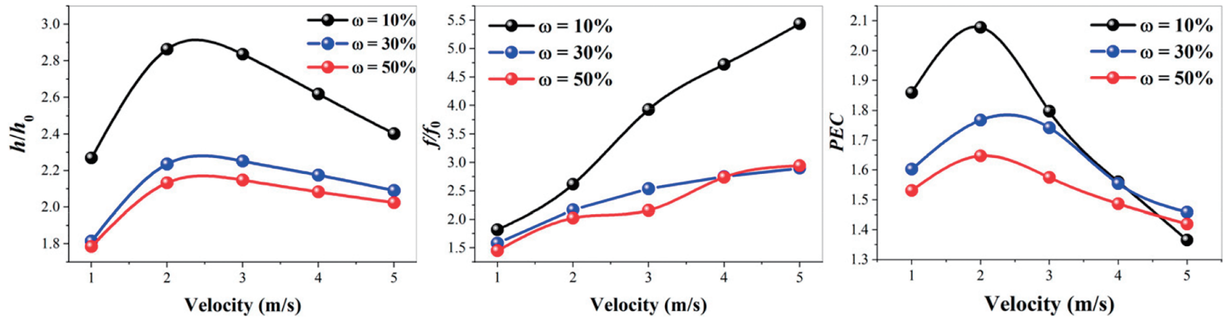

Figure 11: Effects of air mole fraction on thermos-hydraulic performance

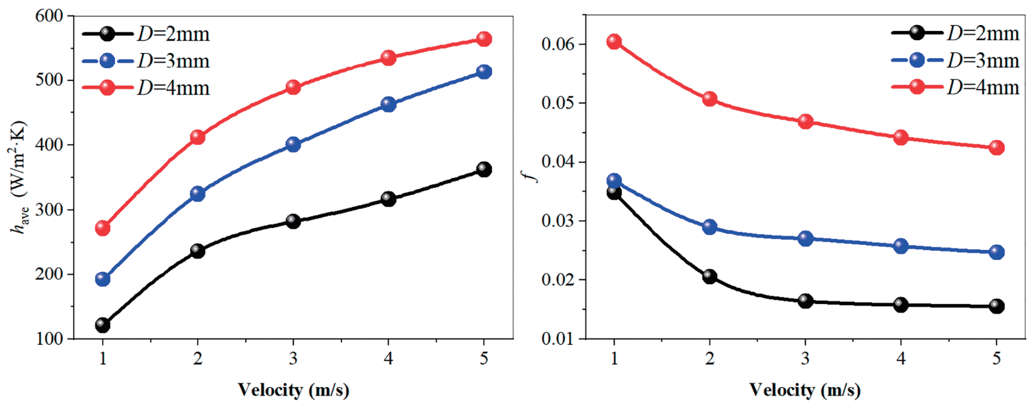

Figure 12: Average heat transfer coefficient and friction factor for different dimple depths

Fig. 13 presents the effects of dimple depth on h/h_0, f/f_0, and PEC. It is observed that the h/h_0 and f/f_0 increase with the rising dimple depth. The range of PEC of the three cases is 1.0–1.61, 1.48–1.97, and 1.36–2.07, respectively. The maximum of PEC is 2.07 in the case of $V = 2$ m/s and $D = 4$ mm.

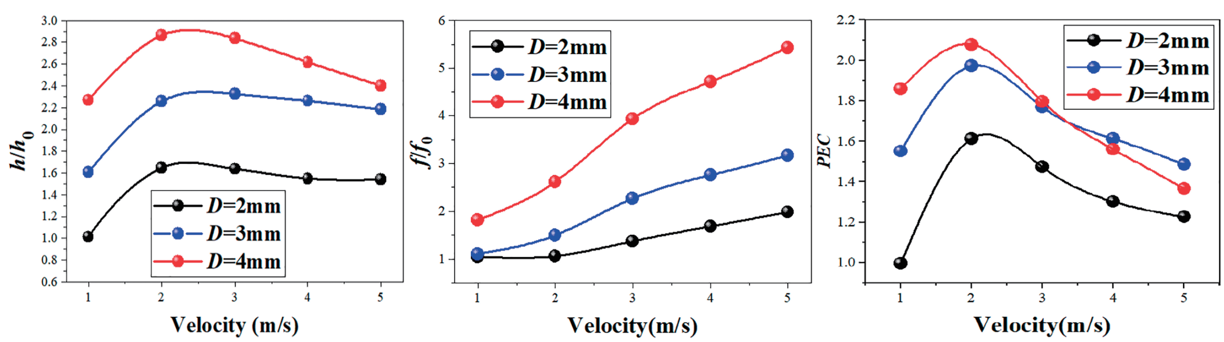

Figure 13: Effects of dimple depth on thermo-hydraulic performance

3.5 *Effect of Dimple Pitch*

Fig. 14 presents the effects of dimple pitch on heat transfer coefficient and friction factor. The heat transfer coefficient and friction factor increase with the declining dimple pitch. When the dimple pitch is relatively small, the turbulence intensity and disruption of the air boundary layer concentration are more drastic. Fig. 15 presents the effects of dimple pitch on h/h_0, f/f_0, and PEC. The h/h_0 and f/f_0 increase with the declining dimple pitch. The PEC of the three cases is 1.60–2.28, 1.36–2.07, and 1.42–1.97, respectively. The PEC of $P = 25$ mm is higher than that of $P = 30$ mm and $P = 35$ mm.

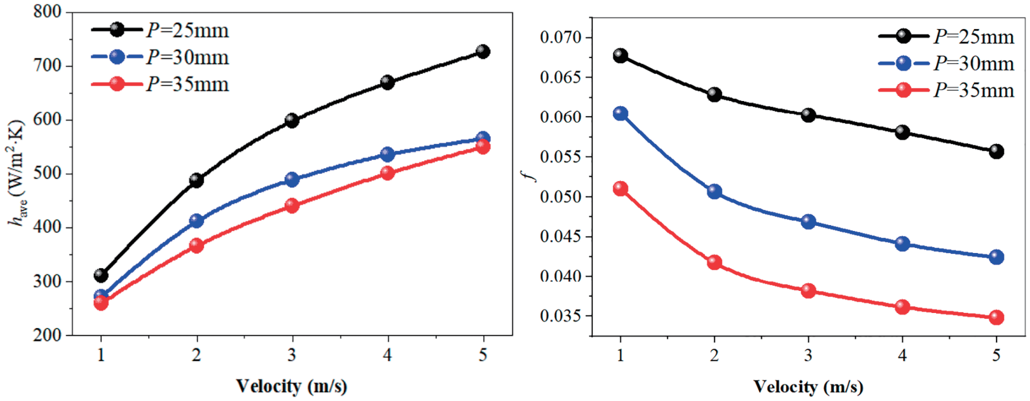

Figure 14: Average heat transfer coefficient and friction factor for different dimple pitches

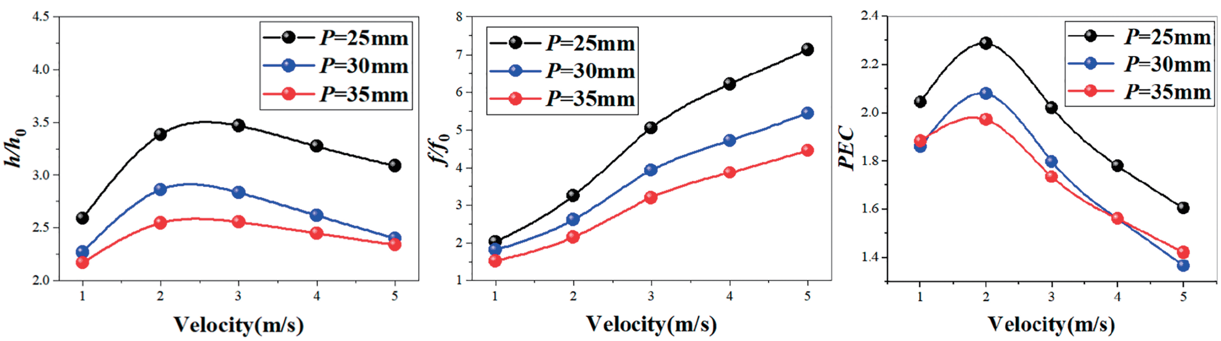

Figure 15: Effects of dimple pitch on thermo-hydraulic performance

4 Conclusions

In this paper, a large deformation-enhanced tube is proposed to improve the condensation heat transfer. A numerical simulation is performed to study the air-steam condensation inside ETDP. In addition, the effects of structure parameters and inlet parameters are discussed. The following conclusions are as follows:

(1) The velocity and temperature fields inside the ETDP present a periodic distribution. The backflow is generated on the leeward side of each dimple, which results in slower flow rates and lower temperatures in these regions. The unique structure of ETDP disturbs the fluid flow near the wall, disrupting the air concentration boundary layer. The distortion of boundary layer flow improves the mixing between the boundary layer flow and the mainstream, resulting in heat transfer enhancement. Compared to the smooth tube, the ETDP significantly improves the heat transfer performance. The heat transfer coefficient is improved by 1.01–3.47 times. The friction factor is improved by 1.05–7.13 times within the scope of the current study.

(2) As the mole fraction of NCG increases, the average heat transfer coefficient decreases, and the friction factor increases. The h/h_0 increases with the rising air mole friction, and the f/f_0 increases with the declining air mole friction. The maximum value of PEC is 2.1 when the air mole friction is 10% and the velocity is 2 m/s.

(3) As the dimple depth increases, the heat transfer performance and friction factor are improved. The disturbance between the boundary layer flow and the mainstream becomes significant. The h/h_0 and f/f_0 increase with the rising dimple depth. The maximum value of PEC is 2.07 when the dimple depth is 4 mm and the velocity is 2 m/s.

(4) The heat transfer coefficient and friction factor increase with the declining dimple pitch. The h/h_0 and f/f_0 increase with the declining dimple pitch. The PEC of $P = 25$ mm is higher than that of $P = 30$ mm and $P = 35$ mm.

Acknowledgement: Not applicable.

Funding Statement: This research was supported by Sichuan Provincial Natural Science Foundation (2024NSFSC0140), Luzhou Science and Technology Project (2022-GYF-15, 2024JYJ073), Intelligent Manufacturing Luzhou Key Laboratory Open Fund (ZZ202405).

Author Contributions: The authors confirm contribution to the paper as follows: Conceptualization and Methodology, Yuanhui Zhang; Software and Data Analysis, Ting Zheng; Resources and Writing—Original Draft, Xuegang Zhang. All authors reviewed the results and approved the final version of the manuscript.

Availability of Data and Materials: All data generated or analyzed during this study are included in this published article.

Ethics Approval: Not applicable.

Conflicts of Interest: The authors declare no conflicts of interest to report regarding the present study.

References

1. Wang X, Zhuo J, Liu J, Li S. Synergetic process of condensing heat exchanger and absorption heat pump for waste heat and water recovery from flue gas. Appl Energ. 2020;261(2):114401. doi:10.1016/j.apenergy.2019.114401.
2. Saeed RM, Schlegel JP, Sawafta R. Characterization of high-temperature PCMs for enhancing passive safety and heat removal capabilities in nuclear reactor systems. Energy. 2019;189(1):116137. doi:10.1016/j.energy.2019.116137.
3. Ayhan H, Sökmen CN. Investigation of passive residual heat removal system for VVERs: effects of finned type heat exchanger tubes. Appl Therm Eng. 2016;108:466–74. doi:10.1016/j.applthermaleng.2016.07.128.
4. Dolatabadi AM, Petruccelli G, Grönman A, Turunen-Saaresti T. A comprehensive numerical investigation of preventing supercritical heat transfer deterioration in the gas heaters of the CO_2 Rankine cycles. Appl Therm Eng. 2025;272(214):126424. doi:10.1016/j.applthermaleng.2025.126424.
5. Petruccelli G, Turunen-Saaresti T, Serret D, Grönman A, Conrozier A, Dolatabadi AM. Experimental and numerical investigation of CO_2 condensation in a printed circuit heat exchanger for transcritical power cycles. Appl Therm Eng. 2025;278:127453. doi:10.1016/j.applthermaleng.2025.127453.
6. Petruccelli G, Momeni Dolatabadi A, Grönman A, Turunen-Saaresti T, Guardone A. Modeling polydispersed droplets in non-equilibrium condensing CO_2 flows through turbine cascades

using moment-based methods for efficient energy utilization. Appl Therm Eng. 2024;256(3):124191. doi:10.1016/j.applthermaleng.2024.124191.

7. Sun F, Yao Y, Li X. The heat and mass transfer characteristics of superheated steam coupled with non-condensable gases in horizontal wells with multi-point injection technique. Energy. 2018;143(9):995–1005. doi:10.1016/j.energy.2017.11.028.
8. Fan G, Tong P, Sun Z, Chen Y. Experimental study of pure steam and steam-air condensation over a vertical corrugated tube. Prog Nucl Energ. 2018;109(7–8):239–49. doi:10.1016/j.pnucene.2018.08.020.
9. Tao LW, Ke MX, Zhi BH, Ming D. Numerical analysis of heat transfer enhancement on steam condensation in the presence of air outside the tube. Nucl Sci Tech. 2022;33(8):100. doi:10.1007/S41365-022-01090-2.
10. Zhang JX, Gong BY. A review about condensation heat tansfer with non-condensable gases. Adv Mater Res. 2012;1791(516–517):239–42. doi:10.4028/www.scientific.net/AMR.516-517.239.
11. Strušnik D, Golob M, Avsec J. Effect of non-condensable gas on heat transfer in steam turbine condenser and modelling of ejector pump system by controlling the gas extraction rate through extraction tubes. Energ Convers Manage. 2016;126:228–46. doi:10.1016/j.enconman.2016.07.082.
12. Di W, Minyang G, Jie C, Guangming F, Jianjun W. Condensation enhancement experiment investigation of pure steam and steam-air mixture over the chrome-plated tube with different plating thickness. Prog Nucl Energ. 2023;166(15):104971. doi:10.1016/J.PNUCENE.2023.104971.
13. Gong LY, Zhao DH, Guo YL, Chen K, Shen SQ. The coupling process of steam condensation and falling film evaporation with non-condensable gas. Int J Therm Sci. 2022;172:107201. doi:10.1016/J.IJTHERMALSCI.2021.107201.
14. Su J, Sun Z, Fan G, Ding M. Experimental study of the effect of non-condensable gases on steam condensation over a vertical tube external surface. Nucl Eng Des. 2013;262:201–8. doi:10.1016/j.nucengdes.2013.05.002.
15. Taehwan A, Jeongmin M, Jinhoon K, Jun JJ, Byongjo Y. Steam condensation in the presence of non-condensable gas inside a nearly horizontal tube under separated flow. Int J Heat Mass Tran. 2022;197(6):123351. doi:10.1016/J.IJHEATMASSTRANSFER.2022.123351.
16. Filip T, Petr K, Jiří P. Heat transfer during condensation of water vapour in the presence of non-condensable gas in vertical tube of small diameter. Case Stud Therm Eng. 2022;40:102519. doi:10.1016/J.CSITE.2022.102519.
17. Lee Y, Jang Y, Kim S. Analysis of air-steam condensation tests on a vertical tube of the passive containment cooling system under natural convection. Ann Nucl Energy. 2019;131:460–74. doi:10.1016/j.anucene.2019.04.001.
18. Zhen X, Xuanyu Z, Shuo K. Experimental study on wet gas condensation heat transfer and flow resistance in horizontal intensified tube. Appl Therm Eng. 2023;230:120742. doi:10.1016/J.APPLTHERMALENG.2023.120742.
19. Qing LH, Hua QC, Xu H, Pin ZL, Gang XC, Li ZH. Investigation on heat transfer performance of corrugated tubes in low-temperature multi-effect falling-film evaporation. Exp Heat Transfer. 2020;34(1):36–50. doi:10.1080/08916152.2020.1713257.
20. Zheng J, Liang Z, Zhang L, Qiu Y, Zhou J, Yan Z. Numerical study on thermo-hydraulic performance of enhanced tube with crossed helical dimples. J Therm Sci Eng Appl. 2023;15(11):111008. doi:10.1115/1.4063044.
21. Zheng J, Liang Z, Zhang L, Zhou J, Yan Z. Forming experiment of extruded tube with crossed ellipsoidal dimples and numerical investigation on heat transfer enhancement and flow characteristics. Int Commun Heat Mass Transf. 2023;141(2):106599. doi:10.1016/j.icheatmasstransfer.2022.106599.
22. Wang H, Abed AM, Al-Zubaidi A, Deifalla A, Galal AM, Zhou Y, et al. Heat transfer enhancement of a copper tube with constant wall temperature using a novel horizontal perforated teardrop-shaped turbulators (PTST). Int J Therm Sci. 2023;192:108418. doi:10.1016/j.ijthermalsci.2023.108418.

23. Xie S, Liang Z, Zhang J, Zhang L, Wang Y, Ding H. Numerical investigation on flow and heat transfer in dimpled tube with teardrop dimples. Int J Heat Mass Transf. 2019;131:713–23. doi:10.1016/j.ijheatmasstransfer.2018.11.112.
24. Yang Z, Shih TH. New time scale based k-ε model for near wall turbulence. AIAA J. 1993;31(7):1191–7. doi:10.2514/3.11752.
25. Li JD. CFD simulation of water vapour condensation in the presence of noncondensable gas in vertical cylindrical condensers. Int J Heat Mass Transf. 2013;57(2):708–21. doi:10.1016/j.ijheatmasstransfer.2012.10.051.
26. Wang X, Chang H, Corradini M. A CFD study of wave influence on film steam condensation in the presence of non-condensable gas. Nucl Eng Des. 2016;305:303–13. doi:10.1016/j.nucengdes.2016.06.003.
27. Bian H, Sun Z, Zhang N, Meng Z, Ding M. Numerical investigations on steam condensation in the presence of air on external surfaces of 3 × 3 tube bundles. Prog Nucl Energy. 2019;111:42–50. doi:10.1016/j.pnucene.2018.10.021.
28. Dong X, Chen W, Cheng Q, Liu Y, Dai H. Numerical analysis of thermal-hydraulic characteristics of steam-air condensation in vertical sinusoidal corrugated tubes. Int J Heat Mass Tran. 2021;164:120558. doi:10.1016/j.ijheatmasstransfer.2020.120558.
29. de la Rosa JC, Escrivá A, Herranz LE, Cicero T, Muñoz-Cobo JL. Review on condensation on the containment structures. Prog Nucl Energy. 2009;51(1):32–66. doi:10.1016/j.pnucene.2008.01.003.
30. Seshadri A, Shirvan K. Development of hydrothermal corrosion model and BWR metal coating for CVD SiC in light water reactors. J Nucl Mater. 2023;576(8):154252. doi:10.1016/J.JNUCMAT.2023.154252.
31. Paul RM, Contescu CI, Gallego NC, Smith R, Bass J, Kane JJ. On the thermal oxidation of nuclear graphite relevant to high-temperature gas cooled reactors. J Nucl Mater. 2023;573:154103. doi:10.1016/J.JNUCMAT.2022.154103.
32. Kuhn SZ, Schrock VE, Peterson PF. An investigation of condensation from steam-gas mixtures flowing downward inside a vertical tube. Nucl Eng Des. 1997;177(1):53–69. doi:10.1016/S0029-5493(97)00185-4.